Broadband reflectance measurements of light penetration, blood oxygenation, hemoglobin concentration, and drug concentration in human intraperitoneal tissues before and after photodynamic therapy

Hsing-Wen Wang
University of Pennsylvania
Department of Physics and Astronomy
209 South 33rd Street
Philadelphia, Pennsylvania 19104-6396
and
University of Pennsylvania
Department of Radiation Oncology
3620 Hamilton Walk
Philadelphia, Pennsylvania 19104-6072

Timothy C. Zhu
University of Pennsylvania
Department of Radiation Oncology
3620 Hamilton Walk
Philadelphia, Pennsylvania 19104-6072

Mary E. Putt
University of Pennsylvania
Department of Biostatistics and Epidemiology
423 Guardian Drive
Philadelphia, Pennsylvania 19104-4209

Michael Solonenko
University of Pennsylvania
Department of Physics and Astronomy
209 South 33rd Street
Philadelphia, Pennsylvania 19104-6396

James Metz
Andreea Dimofte
Jeremy Miles
University of Pennsylvania
Department of Radiation Oncology
3620 Hamilton Walk
Philadelphia, Pennsylvania 19104-6072

Douglas L. Fraker
University of Pennsylvania
Department of Surgery
3400 Spruce Street, 4 Silverstein
Philadelphia, Pennsylvania 19104

Eli Glatstein
Stephen M. Hahn
University of Pennsylvania
Department of Radiation Oncology
3400 Spruce Street, 2 Donner
Philadelphia, Pennsylvania 19104-4283

Arjun G. Yodh
University of Pennsylvania
Department of Physics and Astronomy
209 South 33rd Street
Philadelphia, Pennsylvania 19104-6396
and
University of Pennsylvania
Department of Radiation Oncology
3620 Hamilton Walk
Philadelphia, Pennsylvania 19104-6072

Abstract. We evaluate Photofrin-mediated photodynamic therapy (PDT) in a phase 2 clinical trial as an adjuvant to surgery to treat peritoneal carcinomatosis. We extract tissue optical [reduced scattering (μ_s'), absorption (μ_a), and attenuation coefficients (μ_{eff})] and physiological [blood oxygen saturation ($\%S_tO_2$), total hemoglobin concentration (THC), and photosensitizer concentration ($c_{\text{Photofrin}}$)] properties in 12 patients using a diffuse reflectance instrument and algorithms based on the diffusion equation. Before PDT, in normal intraperitoneal tissues $\%S_tO_2$ and THC ranged between 32 to 100% and 19 to 263 μM, respectively; corresponding data from tumor tissues ranged between 11 to 44% and 61 to 224 μM. Tumor $\%S_tO_2$ is significantly lower than oxygenation of normal intraperitoneal tissues in the same patients. The mean ($\pm$standard error of mean) penetration depth (δ) in millimeters at 630 nm is 4.8($\pm$0.6) for small bowel, 5.2 ($\pm$0.67) for large bowel, 3.39($\pm$0.29) for peritoneum, 5.19($\pm$1.4) for skin, 1.0($\pm$0.1) for liver, and 3.02($\pm$0.66) for tumor. $c_{\text{Photofrin}}$ in micromolars is 4.9($\pm$2.3) for small bowel, 4.8($\pm$2.3) for large bowel, 3.0 ($\pm$1.0) for peritoneum, 2.5($\pm$0.9) for skin, and 7.4($\pm$2.8) for tumor. In all tissues examined, mean $c_{\text{Photofrin}}$ tends to decrease after PDT, perhaps due to photobleaching. These results provide benchmark *in-vivo* tissue optical property data, and demonstrate the feasibility of *in-situ* measurements during clinical PDT treatments. [DOI: 10.1117/1.1854679]

Keywords: photodynamic therapy; peritoneal carcinomatosis; *in-vivo* intraperitoneal optical properties; physiological properties; diffuse reflectance spectroscopy; photodynamic therapy dosimetry.

Paper 04037 received Mar. 15, 2004; revised manuscript received Jun. 21, 2004; accepted for publication Jun. 28, 2004; published online Feb. 10, 2005.

1 Introduction

Photodynamic therapy (PDT) is a cancer treatment approved by the U.S. Food and Drug administration (FDA) for treatment of obstructing esophageal and lung cancers, and for microinvasive lung cancers.[1] PDT is also an attractive treatment for superficial lesions[2] such as skin cancers,[3–6] carcinoma *in-situ* of the upper aerodigestive tract,[7–9] and as an adjuvant to surgical debulking of serosal tumors such as pleural[10–12] and peritoneal malignancies.[13–15] Currently, no curative therapy exists for the disseminated intraperitoneal cancers. At the University of Pennsylvania we are evaluating Photofrin-mediated PDT in patients with intraperitoneal (IP) malignancies in a phase 2 clinical trial. We report *in-vivo* measurements of the tissue optical and physiological properties of patients enrolled in this trial.

PDT efficacy depends on concentrations of photosensitizer and oxygen in patient tissues, and on light delivery.[1,16] The photoexcited sensitizer initiates a cascade of chemical reactions to form either oxidized products (type 1 reaction) or singlet oxygen (type 2 reaction), leading to direct cytotoxicity or vascular damage, and subsequently, to tumor regression. Oxygen is therefore a critical component of clinical PDT.[17–19] In addition, optical properties of tissues such as their absorption $\mu_a(\lambda)$ and reduced scattering $\mu_s'(\lambda)$ coefficients influence tissue light dose and affect PDT.[20] Finally, the distribution of a photosensitizer within target tissues impacts outcome. The availability of photosensitizer, light, and oxygen and their relationship in time and space determines the efficacy of PDT.

In contrast to the highly sophisticated treatment planning used, for example, in ionizing radiation therapy, PDT dosimetry and treatment planning is still in its infancy. Most current FDA-approved clinical protocols do not employ light, oxygen, or photosensitizer dosimetry. Even in clinical research protocols, only light dose is measured *in situ*; tissue optical properties are neither measured nor incorporated into treatment planning. Desirable ingredients for PDT dosimetry and treatment planning include *in-situ* measurement of light dose, measurement of tissue oxygen, and quantitative measurement of photosensitizer. When implemented properly, this information enables determination of explicit and implicit dose factors affecting PDT,[21] and supports further development of concrete theoretical models of PDT mechanisms.

Near-infrared spectroscopy (NIRS) and NIR diffuse optical tomography (DOT) have emerged as important techniques to obtain tissue optical properties noninvasively.[22] The intrinsic absorption sensitivity to these optical methods makes them particularly attractive for measurement of tissue chromophores such as oxy-hemoglobin, deoxy-hemoglobin, tissue parameters such as hemoglobin oxygen saturation, total hemoglobin concentration, as well as the concentration of other chromophores such as lipid, water, and photosensitizer. As a result there have been many investigations of *in-vivo* optical properties in animal organs[23–28] and in humans.[29–43] However, there have been relatively few human tissue studies during or after PDT.[44–49]

Address all correspondence to Dr. Hsing-Wen Wang, Univ. of Pennsylvania, Department of Physics and Astronomy, 209 S. 33rd Street, Philadelphia, PA 19104-6396. Tel: 215-573-6404; E-mail: hwwang@physics.upenn.edu

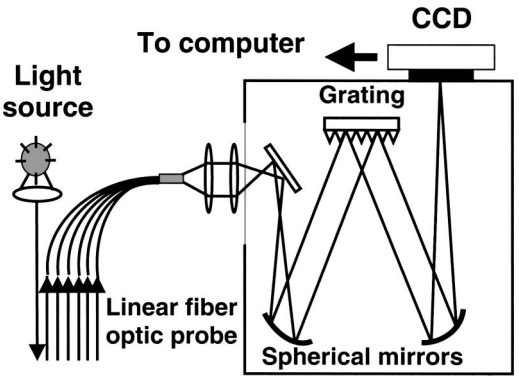

Fig. 1 Schematic diagram of a broadband reflectance spectrometer consisting of a halogen white light source, fiber optic probe, monochromator, and liquid nitrogen-cooled CCD camera.

We have measured the optical properties of 12 patients with intraperitoneal malignancies as part of an on-going PDT trial using our broadband reflectance spectroscopy system.[50] The measurements were performed with continuous wave (cw) NIRS instrumentation over a wide spectral range (600 to 800 nm), before and after PDT treatment among various organs. To our knowledge, this is the first report of noninvasive optical property measurement in human intraperitoneal tissue. We have determined light penetration depth, blood oxygen saturation, total hemoglobin concentration, and drug concentration of normal and cancerous tissues. This investigation, therefore, takes a first step toward improving PDT dosimetry; we characterize the heterogeneity of these quantities with respect to location, tissue type, and patient, and we explore how these properties change as a result of PDT treatment.

2 Methods

2.1 *Instrument and Calibration*

Our broadband reflectance spectrometer system[50] is based on recently developed optical instrumentation.[51] The original design principle is due to Wilson, Farrell, and Patterson.[52] A schematic diagram of the system is shown in Fig. 1. The system has four major parts: light source, fiber optic probe head, dispersion system (monochromator), and charge-coupled device (CCD) camera. We simultaneously collect tissue reflectance spectra at many source-detector separations.

Briefly, light from a 250-W quartz tungsten halogen lamp (Cuda Fiberoptics, Jacksonville, Florida) was coupled to the tissue surface through the source optical fiber. Diffuse light reflected back from the tissue surface was collected by a linear array of detector fibers. Light from the detector fibers was then coupled to the entrance slit of a monochromator (Acton Research, Acton, Massachusetts). The detector fibers were arranged in a vertical line within the entrance slit, with equal spacing. The fiber tips were imaged through the monochromator, and onto a liquid nitrogen-cooled CCD camera sensor (Roper Scientific, Trenton, New Jersey). The grating dispersed the fiber output light, creating a series of vertically spaced bright strips in the image plane of the monochromator

1083-3668/2005/$22.00 © 2005 SPIE

(i.e., at the CCD). Each strip represented the spectrum $R_{\text{tissue}}(\rho,\lambda)$ dispersed from a single detection fiber with source-detector separation distance ρ. The average spectrum was obtained by binning vertically over 27 to 35 pixels.

The nitrogen-cooled CCD camera contained 330 (vertical) $\times$1100 (horizontal) pixels (24 μm) spread over an 8$\times$26 mm area. The pixel noise was $<$1 electron/s at 173 K, and the CCD quantum efficiency was 35% at 700 nm. The spectral resolution was approximately 0.5 nm/pixel for our grating (300 groves/mm). We typically set the central wavelength to 620 or 700 nm, and we collected spectra in the 380 to 880 nm or 450 to 950 nm ranges, respectively. The integration time for measurements was approximately 100 ms.

We used two linear fiber optic probe heads for the IP-PDT clinical data. One probe consisted of a source fiber and six detection fibers, each with 600-μm core diameter. The source-detector separation distance ρ ranged from 1.3 to 7.8 mm; detection fibers were equally spaced. A second probe was similar, except the fiber core diameters were 400 μm and the ten detection fibers were spaced nonuniformly with source-detector separation ranging from 0.6 to 10 mm.

To account for the spectral features of the white light source and the optical throughput of our detection system, we took additional measurements immediately after each clinical study using a 6-in.-diam integrating sphere (LabSphere, Incorporated, North Sutton, New Hampshire). A single optical fiber, coupling light from the same light source, illuminated the integrating sphere through its 0.5-in.-diam opening; the fiber optic probe head was placed in the other opening of the integrating sphere to collect a calibration signal $R_{\text{sphere}}(\rho,\lambda)$. An effective measured reflectance $R_{\text{measured}}(\rho,\lambda)$ was then calculated as:

$$R_{\text{measured}}(\rho,\lambda)=\frac{R_{\text{tissue}}(\rho,\lambda)-B_{\text{tissue}}(\rho,\lambda)}{R_{\text{sphere}}(\rho,\lambda)-B_{\text{sphere}}(\rho,\lambda)}. \quad (1)$$

Here, $B_{\text{tissue}}(\rho,\lambda)$ and $B_{\text{sphere}}(\rho,\lambda)$ are background spectra collected with the light source off.

2.2 *Patients and Clinical PDT Treatments*

All patients were enrolled in the phase 2 study of intraperitoneal PDT conducted at the Hospital of University of Pennsylvania. The primary endpoint of this study was to evaluate the effectiveness of debulking surgery and adjuvant intraperitoneal photodynamic therapy utilizing Photofrin II. Patients with ovarian cancer, sarcoma, or gastrointestinal malignancies were enrolled in the study, and the protocol was amended to include measurements of optical properties intraoperatively. All patients signed a study-specific informed consent. The protocol was approved by the University of Pennsylvania Institutional Review Board and the Clinical Trial Scientific Review and Monitoring committee of the University of Pennsylvania Cancer Center. The protocol was conducted under an investigator-sponsored investigational new drug application (IND) with the U.S. Food and Drug Administration.

Treatment details for intraperitoneal PDT are described elsewhere.[14,15] Briefly, patients received Photofrin (2.5 mg/kg) administered intravenously (IV) approximately 48 h before surgery. Surgery consisted of debulking of all gross tumors to a maximal residual thickness of 5 mm or less. Six sterile photodiodes were placed in the right upper quadrant, left upper quadrant, right paracolic gutter, left paracolic gutter, and midline pelvis to monitor light delivery *in situ*. The small and large bowel, and mesentery were treated with 532-nm green light using a flat-cut fiber; dose was monitored with a mobile flat diode. The rest of the abdomen was then treated with 630 nm light. Prior to 630 nm light treatment, the peritoneal cavity was filled with an Intralipid solution (0.01%), which scattered light and maximized light delivery to the peritoneal cavity. Light was delivered to all surfaces of the abdominal cavity by using an optical fiber sheathed within a modified endotracheal tube (balloon cuff inflated and filled with dilute Intralipid).

The cw absorption probe was sterilized prior to surgery. Before and immediately after PDT treatment, the physician placed the contact probe head on the tissue surface and then optical property measurements were taken. To minimize patient time in the operation room, one measurement was taken from each organ of each patient (with the exception of some tumor tissues). Measurements reported here were taken from normal tissues including small bowel, large bowel, peritoneum, skin (adjacent to the surgical incision), and liver, as well as from tumor tissue.

2.3 *Theory and Analysis of Optical Data*

Biological tissues such as these are often modeled as homogeneous turbid media with scatterers and absorbers. Photons diffuse in such turbid media and their transport are reasonably well described by a diffusion equation, i.e.,

$$\frac{\partial\Phi(\vec{r},t)}{\partial t}=\nabla\cdot D\nabla\Phi(\vec{r},t)-v\mu_a\Phi(\vec{r},t)+vS(\vec{r},t). \quad (2)$$

Here, $\Phi(\vec{r},t)$ is the photon fluence rate, in units of photons per cm^2 per second; c is the vacuum speed of light, and v is the speed of light in the turbid medium having refractive index n such that $v=c/n$; $D=v/[3(\mu_s'+\mu_a)]$ is the photon diffusion coefficient; $\mu_a(\lambda)$ and $\mu_s'(\lambda)$ are absorption and reduced scattering coefficients, respectively; and S is an isotropic source term that gives the number of photons emitted at position $\vec{r}$ and time t, per unit volume per unit time.

In our measurement scheme, source and detector fibers reside on the same tissue surface, separated by distance ρ along that surface. The tissue sample is then modeled as a semi-infinite medium. The diffuse reflectance is $R[\rho,\mu_a(\lambda),\mu_s'(\lambda)]$. The solutions for $R[\rho,\mu_a(\lambda),\mu_s'(\lambda)]$ from semi-infinite media with steady-state excitation are well known:[51,53–57]

$$R[\rho,\mu_a(\lambda),\mu_s'(\lambda)]=C_1\Phi(\rho)+C_2 j_z(\rho),$$

$$\Phi(\rho)=\frac{1}{4\pi D}\left[\frac{\exp(-\mu_{\text{eff}}r_1)}{r_1}-\frac{\exp(-\mu_{\text{eff}}r_2)}{r_2}\right],$$

$$j_z(\rho)=\frac{1}{4\pi}\left[\frac{1}{\mu_t'}\left(\mu_{\text{eff}}+\frac{1}{r_1}\right)\frac{\exp(-\mu_{\text{eff}}r_1)}{r_1^2}+\left(\frac{1}{\mu_t'}+2z_b\right)\times\left(\mu_{\text{eff}}+\frac{1}{r_2}\right)\frac{\exp(-\mu_{\text{eff}}r_2)}{r_2^2}\right]. \quad (3)$$

where $\Phi(\rho)$ and $j_z(\rho)$ are photon fluence and flux rate, respectively, and are functions of ρ, $\mu_s'(\lambda)$, and $\mu_a(\lambda)$. The parameters z_b, r_1, and r_2 are derived from the extrapolated boundary conditions.[54] C_1 and C_2 are constants that depend on the relative refractive indices of tissues and detection fibers, and on the numerical aperture of the detection fibers.[51]

The fidelity of our measurements is improved substantially because we use many optical wavelengths. For analysis we employed a multiwavelength algorithm that simultaneously fits all reflectance spectra in the wavelength range of 600 to 800 nm using multiple source-detector separation distances. To extract $\mu_s'(\lambda)$ and $\mu_a(\lambda)$, we have made two additional assumptions about $\mu_s'(\lambda)$ and $\mu_a(\lambda)$ that stabilize the analysis even more: 1. $\mu_a(\lambda)=\Sigma_i c_i \epsilon_i(\lambda)$, and 2. $\mu_s'(\lambda)=A\lambda^{-B}$.[30,50,58] Here, $\epsilon_i(\lambda)$ is the molar spectral absorbance (or the extinction coefficient) of the i'th chromophores, and c_i is equivalent to the molar concentration of the i'th chromophore. The major chromophores in the spectral range of 600 to 800 nm are oxy- (HbO_2), deoxy-hemoglobin (Hb), water, and Photofrin. We obtained the extinction coefficient of oxy-, deoxy-hemoglobin, and water from the literature,[59] and that of Photofrin by direct measurement using an absorption spectrometer. The approximation $\mu_s'(\lambda)=A\lambda^{-B}$ has been shown to follow from the Mie theory over our spectral range, and thus simulates tissue scattering reasonably well.[30,31,60,61]

We directly reconstructed the concentrations c_{HbO2}, c_{Hb}, c_{water}, and $c_{\mathrm{Photofrin}}$, and the parameters A and B using a nonlinearly constrained optimization method, FMINCON, implemented in MATLAB (The MathWorks, Incorporated, Natick, Massachusetts). We constrained the upper and lower boundaries for each extracted quantity i.e., $0 \leqslant A \leqslant 107$, $0 \leqslant B \leqslant 3$, $0 \leqslant C_{\mathrm{HbO2}}$, $C_{\mathrm{Hb}} \leqslant 500$ μM, $0 \leqslant c_{\mathrm{Photofrin}} \leqslant 40$ μM, and $0 \leqslant c_{\mathrm{water}} \leqslant 1$. The scheme minimizes χ^2,

$$\chi^2=\sum_{\rho}\sum_{\lambda}\left|\frac{R_{\mathrm{measured}}(\rho,\lambda)}{R_{\mathrm{measured}}(\rho=\rho_0,\lambda)}-\frac{R_{\mathrm{calculated}}(\rho,\lambda)}{R_{\mathrm{calculated}}(\rho=\rho_0,\lambda)}\right|^2. \tag{4}$$

Here, we have normalized both $R_{\mathrm{measured}}(\rho,\lambda)$ and $R_{\mathrm{calculated}}(\rho,\lambda)$ to the spectrum of one source-detector separation distance ($\rho_0=1.3$ mm for the six detector fiber probe and $\rho_0=1.2$ mm for the ten detector fiber probe), respectively, before fitting. We define fitting error ξ as $\xi=\sqrt{\chi^2}/N$, where N is the data size in order to compare the fitting performances of tissue phantoms and tissue samples.

At each separation distance, there are 441 data points with spectral resolution 0.4545 nm/pixel. To save calculation time, we used half of the dataset (221 data points) with spectral resolution 0.9091 nm/pixel for processing. The number of separation distances employed determined the final number of data points used for fitting. We reoptimized the combination of separation distances for each sample for two reasons: signal-to-noise degraded at large separation distances, and tissue heterogeneities (on the surface and below the surface) sometimes altered fitting performance. The source detector separation distances used in our analysis were typically between 1 and 5.2 mm. We also empirically found that data from the $\rho=0.6$ mm separation in the 10 detector probe introduced a large error while fitting. Therefore, we excluded this detector from our analysis. The typical processing time for analysis of each clinical measurement is less than 3 s on a 700-MHz Pentium III processor.

Using the reconstructed parameters A, B, and c_i, we obtained $c_{\mathrm{Photofrin}}$ directly and calculated $\mu_s'(\lambda)$, $\mu_a(\lambda)$, attenuation coefficients $[\mu_{\mathrm{eff}}(\lambda)=\sqrt{3\mu_s'\mu_a}]$, penetration depth $[\delta(\lambda)=1/\mu_{\mathrm{eff}}(\lambda)]$, total hemoglobin concentration ($c_{\mathrm{HbO2}}+c_{\mathrm{Hb}}$), and tissue blood oxygenation $[c_{\mathrm{HbO2}}/(c_{\mathrm{HbO2}}+c_{\mathrm{Hb}})]$. We report μ_s', μ_a, μ_{eff}, and δ at 630 nm because it is the treatment wavelength for Photofrin. Optical properties at other wavelengths between 600 and 800 nm can be calculated from these data as well. Water content was not reported in this study because its value was relatively insensitive to the fitting performance of the multiwavelength algorithm. This is probably because of its low absorption in the 600 to 800 nm spectral range. Data from tissue phantoms were used for validating the instrument and algorithm, and are reported as mean, ± standard deviation (SD), ± standard errors of the mean (SEM, the SD divided by the square root of the number of observations or sample size n), and the coefficient of variation (CV, the standard deviation divided by the mean). Accuracy is defined here as the measured value divided by the true value.

2.4 *Statistical Analysis of Clinical Data*

For the clinical study, measurements were collected on 12 patients. Duplicate measurements from the same tissue were averaged prior to analysis. However, issues related to patient care prevented us from taking measurements on all tissues at both before and after PDT time points, and from both tumor and normal tissues for all patients. To compare results from different normal tissues, only data from those patients receiving measurements in all tissues before or after PDT were analyzed. To compare results before and after PDT, ratios were formed for individual patients receiving measurements in a specific tissue both before and after PDT. Similarly, tumor-to-normal tissue ratios of each parameter of interest were formed for each individual and used in the analysis. Statistical analyses were carried out using the freeware R 1.7.0.[62]

Because, to our knowledge, this is the first report of data of this type, we graphically present the data for individual patients, and we provide summaries of the data, i.e., medians and or means, together with either the SEM, standard error of the mean, or a 95% confidence interval (95% CI) on the mean, and number of patients n. The confidence intervals were based on the T distribution and the estimated SEMs; if a 95% confidence interval did not cover a hypothesized value, e.g., value 1.0 for a mean of a ratio, then it indicates that the means were significantly different from the hypothesized value. Similarly, if the p-value for a test was smaller than a type 1 error rate of 0.05, we declared the test to be statistically significant. All hypothesis tests were two-sided. Friedman's test, a nonparametric analog of a repeated measures analysis of variance, was used to determine whether there were significant differences in each optical and physiological property between at least one pair of normal tissue types.[63] If significant differences were found, then a paired t-test was used to make pairwise comparisons among the tissues. By using a global test for each parameter of interest (Friedman's test) followed by a pairwise test in cases where the global test

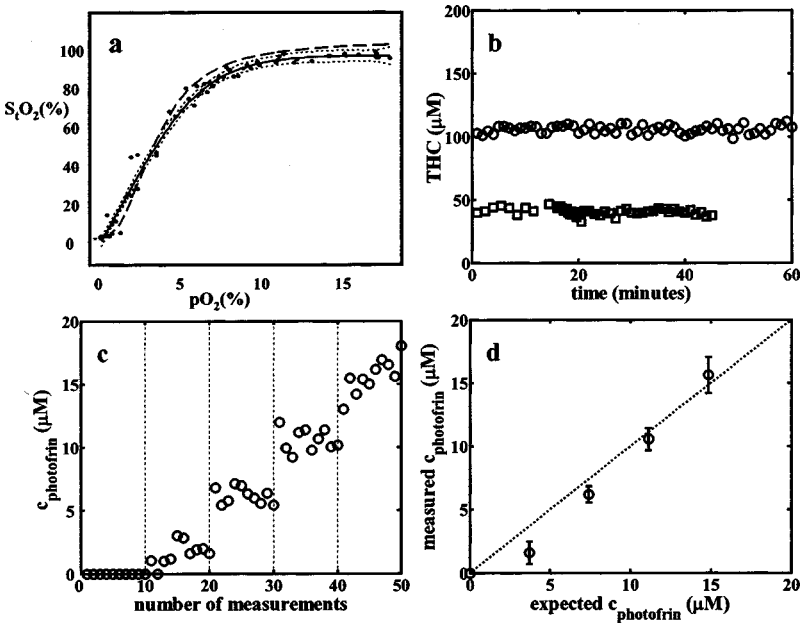

Fig. 2 Measured tissue blood oxygenation (%S_tO_2), total hemoglobin concentration (THC), and Photofrin concentration ($c_{Photofrin}$) in hemoglobin phantoms using broadband reflectance spectroscopy. (a) %S_tO_2 was plotted versus electrode probe measured oxygen partial pressure (pO_2). The solid line was fit to the data using an optimal P-spline. Dotted lines are approximately 95% confidence intervals on the mean fit. A human blood dissociation curve (dashed line) was plotted for comparison. (b) THC was measured at 50 (□) and 100 μM (○) and plotted versus time. (c) Individual measurements in the hemoglobin phantom with five different Photofrin concentrations were plotted versus the number of measurements. Ten measurements were taken at each Photofrin concentration. (d) The mean and standard deviation of measured Photofrin concentrations were plotted versus the true concentration. The measurements underestimated the true concentration at lower concentration (<5 μM), but are accurate otherwise.

achieves statistical significance, we reduced the number of tests used in the analyisis. Thus in Table 2, 46 pairwise tests out of 96 possibilities were constructed. By using this approach, we hoped to reduce the number of false positive tests.

To compare parameters before versus after PDT, we did not preceed our pairwise tests with a global test because of certain parameters (e.g., Photofrin concentration), the number of patients with measurements in all tissues was too small to carry out the test. Descriptive statistics (means of ratios and their associated 95% CIs) and hypothesis tests (paired T-test) for these ratios were based on log-transformed data. Because measured concentrations of Photofrin were zero in some tissues, differences instead of ratios were used to analyze these data, and the data were not log transformed. If the lower endpoint of a 95% CI was negative, it was truncated to zero if a negative value was meaningless.

2.5 *Validation of the Instrument and the Algorithm with Tissue Phantoms*

We validated the stability and accuracy of our instrument and the global algorithm using tissue-simulating phantoms. Three types of phantom were used. One was a scattering phantom, Intralipid (IL) at various concentrations to validate μ_s'. A second phantom was a mixture of hemoglobin (human blood) and Intralipid to validate the physiological properties of total hemoglobin concentration (THC) and blood oxygen saturation (%S_tO_2). Finally, Photofrin was added into the hemoglobin phantom to validate Photofrin concentration. A magnetic stirring rod was used during the phantom studies to insure solution uniformity.

A 30% Intralipid solution was diluted to 0.5, 1, 1.5, and 2%. The solution had $\mu_s'=5$, 10, 15, and 20 cm^{-1} at 830 nm, respectively, according to Mie theory approximations,[60] which predict that μ_s' of 10% Intralipid is given by $\mu_s'=\mu_s(1-g)\,[cm^{-1}]$, with $\mu_s=(2.54\times10^9)(\lambda\,[nm]^{-2.4})\,[cm^{-1}]$ and $g=1.1-(0.58\times10^{-3})(\lambda\,[nm])$. Then, the μ_s' of X% Intralipid was calculated using the relation $\mu_s'^{X\%IL}\times V^{X\%IL}=\mu_s'^{10\%IL}\times V^{10\%IL}$ for given volumes (V) of 10% Intralipid and X% Intralipid and $\mu_s'^{10\%IL}$. The results from ten measurements at each Intralipid concentration show that the measurement coefficient of variance (CV) was typically less than 0.3% and the measurement accuracy was 135, 106, 105, and 101% for 0.5, 1, 1.5, and 2% IL, respectively. The reconstructed μ_s' for the lower concentration solution (i.e., $\mu_s'\leqslant5$ cm^{-1} at 830 nm) was clearly overestimated.

In the hemoglobin phantoms, we simultaneously monitored the oxygen partial pressure (pO_2) by using a Clark-type electrode probe. After adding fresh human blood into the 1% Intralipid and waiting until a pO_2 equivalent to air oxygen concentration (21% or 159.6 Torr) was achieved, the sample oxygenation was decreased by pumping nitrogen gas into the phantom solution continuously. Optical and partial pressure measurements were taken in intervals that varied from 30 s to 5 min depending on the speed of pO_2 variation. The measured blood oxygen saturation (%S_tO_2) is plotted versus pO_2 in Fig. 2(a). The data were fit to a solid line in Fig. 2(a) using an optimal P-spline with 95% confidence intervals (dotted lines) shown.[64] The oxygen dissociation curve or Hill curve of human blood[51] is also shown in the same figure for comparison

Table 1 Number of patients on whom optical property measurements were performed in various organs before and after PDT. Nine tumor tissues were collected from the six tumor patients before PDT.

Condition	Small bowel	Large bowel	Peritoneum	Tumor	Skin	Liver
Before PDT	12	9	10	6	11	10
After PDT	8	5	7	0	6	5

(dashed line). Compared to this Hill curve, the fitted curve suggests $\%S_tO_2$ is slightly overestimated at low pO_2, and slightly underestimated at high pO_2. However, the difference between the smoothed fit and the theoretical values (Hill curve) is less than 5%.

The stability and accuracy of total hemoglobin concentration (THC) measurements were determined from similar hemoglobin phantoms having 0.8% IL and two different THC concentrations of 50 and 100 μM, respectively, as shown in Fig. 2(b). The mean values ($\pm$SD) from 50 to 60 repeated measures of THC were 44.8$\pm$1.3 and 111.5$\pm$3.5 μM with a corresponding coefficient of variation (CV) of 2.9% and 3.2% and an accuracy of 110.4% and 111.5%, respectively. The stability of $\%S_tO_2$, μ_s', μ_a, and μ_{eff} was also validated in the hemoglobin phantom with THC 100 μM. The mean values ($\pm$SD) of $\%S_tO_2$ and μ_s', μ_a, and μ_{eff} at 630 nm were 70.5%$\pm$1.2%, 12.1$\pm$0.07 cm^{-1}, 0.216$\pm$0.003 cm^{-1}, and 2.824$\pm$0.013 cm^{-1} with corresponding CVs 1.7, 0.6, 1.3, and 0.6%, respectively.

Figures 2(c) and 2(d) show the results of measuring Photofrin concentration in the hemoglobin phantom (THC 50 μM, 0.8% IL). Photofrin was increased from 0 to 15 μM (corresponding to 7.5 mg/kg, assuming the molecular weight of Photofrin is 500) with increments of 3.7 μM. At each concentration, ten measurements were performed [Fig. 2(c)] and the measured mean values ($\pm$SD) are 1.6$\pm$0.9, 6.2$\pm$0.6, 10.6 $\pm$0.9, and 15.6$\pm$1.4 μM, respectively, with corresponding coefficients of variation (CVs) of 56, 9.7, 8.5, and 9.0%, respectively [Fig. 2(d)]. Overall, the values of measured Photofrin concentration fluctuated more than other optical and physiological properties. Photofrin concentration was also underestimated at low true Photofrin concentration (=3.7 μM). However, the values of other optical (μ_s', μ_a, and μ_{eff}) and physiological properties (THC and $\%S_tO_2$) were measured to stay constant (within measurement stability) during the entire experiment (data not shown).

3 Results

In-vivo optical property measurements of normal and tumor tissues were made on 12 patients enrolled in the study between November 2000 and August 2002. Measurements were made for normal tissues from the small and large bowel, peritoneum, liver, and skin, and from tumors. Table 1 summarizes the number of patients with measurements for each tissue. Measurements were made both before and after PDT.

3.1 *Algorithm Performance in Clinical Data*

The performance of the fitting between measured and calculated spectra is shown in Fig. 3. Figure 3(a) shows the normalized plot of measured and calculated diffuse reflectance spectra from large bowel, as an example, using the six-detector probe. The source-detector separation distances used in this case to extract the optical and physiological parameters were 1.3, 2.6, 3.9, and 5.2 mm. The reconstructed diffuse reflectance spectra were back calculated based on Eq. (3) by applying the algorithm outputs $A=1499.5$, $B=0.8423$, $c_{\text{HbO2}}=122.42\,\mu$M, $c_{\text{Hb}}=37.25\,\mu$M, and $c_{\text{Photofrin}}=4.3\,\mu$M. The fitting error ξ (defined previously) is 7.1%. To compare the fitting performance in human tissues and tissue phantoms, Fig. 3(b) shows a similar plot from a hemoglobin phantom using a similar range of source-detector separation distances (1.2, 1.8, 2.4, 3, 4, 5, and 6 mm) of the ten-detector probe. The fitting error is 2.3% in tissue phantom, three times less than in the large bowel tissue sample. These differences could have arisen from a variety of factors that are difficult to know and/or control including tissue heterogeneity.

3.2 *Between and Within Patient Heterogeneity*

Variation in μ_s', μ_a at 630 nm, and THC, all measured before PDT in three intraperitoneal tissues, is shown both between individual patients and within patients (Fig. 4). Patients with complete data on all five sites where optical measurements were collected (C1 to C7) are distinguished from those with incomplete data on at least one site (I1 to I5). The plot shows the variability in $\%S_tO_2$ before PDT for six patients with complete data on all five sites (C1 to C6) and for six patients with incomplete data on at least one site (I1 to I6). For patients with complete data, the normal intraperitoneal tissues have $\%S_tO_2$ in the range of 32 to 100% and a THC in the range of 19 to 263 μM.

Within the intraperitoneal tissues before PDT, substantial heterogeneity was observed between individual patients in μ_s', μ_a at 630 nm, $\%S_tO_2$, and THC. For example, median values of μ_s' ranged from 6.2 cm^{-1} for C4 to 22.9 cm^{-1} for I2, and the median values of $\%S_tO_2$ ranged from 51.8% for C6 to 97.3% for C5. The range of measurements for μ_s', μ_a at 630 nm, and THC within patients was highly variable as well. For example, values of μ_s' for patient C4 ranged from 4.9 to 6.6 cm^{-1}, while μ_s' for patient I2 ranged from 13.5 to 47.6 cm^{-1}.

3.3 *Differences among Normal Tissues*

The means ($\pm$SEM) of optical properties (μ_s', μ_a, and μ_{eff} at 630 nm) and physiologic parameters ($\%S_tO_2$, THC, and $c_{\text{Photofrin}}$) and their corresponding sample sizes for five different normal tissues (small and large bowel, peritoneum, skin, and liver) before and after PDT are listed in Table 2. In the pre-PDT measurements, Friedman's test for each optical property, μ_s', μ_a, and μ_{eff}, showed evidence of statistically significant differences among at least one pair of the five tissues. Mean values for liver were substantially higher than for all other tissues, with skin and peritoneum somewhat higher than small and large bowel. In pairwise comparisons, differences between liver and other tissues were consistently significant. In addition, for μ_{eff}, means for small and large bowel were significantly smaller than for peritoneum.

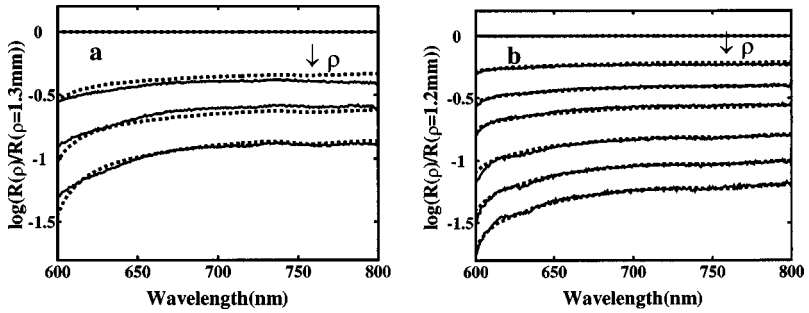

Fig. 3 Measured (—) and calculated (----) reflectance spectra at ρ=1.3, 2.6, 3.9, and 5.2 mm in (a) a normal large bowel tissue sample and at (b) ρ=1.2, 1.8, 2.4, 3, 4, 5, and 6 mm hemoglobin phantom, after normalized to the spectrum at ρ=1.3 and 1.2 mm, respectively. The spectra from top to bottom denote the increasing values of ρ (as indicated in arrows). The calculated reflectance spectra were calculated based on the output values of the global algorithm that $A=1499.5$, $B=-0.8423$, $c_{HbO2}=122$ μM, $c_{Hb}=37$ μM, and $c_{Photofrin}=10$ μM for the large bowel tissue sample, and $A=1500.5$, $B=-0.7801$, $c_{HbO2}=32$ μM, $c_{Hb}=21$ μM, and $c_{Photofrin}=15$ μM for the hemoglobin phantom. The tissue sample shows a larger fitting error (ξ=7.1%), defined in the text, than tissue phantom (ξ=2.3%) as expected.

Qualitatively, the trends in optical properties were similar in post-PDT measurements, although measurements were collected on fewer subjects. Mean values for liver were consistently higher than for other tissues, with peritoneum and skin for μ_s' and μ_{eff} tending to be higher than small and large bowel. Friedman's test indicated that differences between at least one pair of tissues were statistically significant for μ_s' and μ_{eff}. With the exception of μ_s' in skin, pairwise differences in mean values for liver and all other tissues were consistently significant for μ_s' and μ_{eff}.

For the comparison of physiological properties, liver was omitted from the analysis because we were unable to extract the oxygenation and THC information from liver tissues in our current analytical model. The diffusion model breaks down at high absorption ($\mu_a/\mu_s'>0.1$), wherein the ratio of absorption to scattering is large; the optical properties of liver fall in this range. For the comparison of Photofrin concentration among tissues, skin was also omitted for the same reason. For the other tissues, data were available for between five and seven patients before PDT, and for three patients after PDT. Friedman's test did not find any significant differences in the distribution of physiological properties among tissues except for $\%S_tO_2$ before PDT. Pairwise tests indicated that means of $\%S_tO_2$ for large bowel were significantly higher than peritoneum and skin, and approached statistical significance for small bowel as well (P=0.065).

3.4 *Differences in Normal Tissue before Versus after PDT*

Because of the large amount of variability among patients, differences in optical and physiologic parameters before versus after PDT were analyzed only for patients who had both measurements for the parameter of interest. Table 3 shows the mean of the individual ratios (95% CI) of optical properties, $\%S_tO_2$, and THC before versus after PDT. The concentration of Photofrin was sometimes measured as zero before or after PDT. Instead of calculating ratios, the mean difference in Photofrin concentration before versus after PDT was reported in Table 3. For the optical properties, and for $\%S_tO_2$, the mean of the individual ratios were qualitatively similar to 1.0 and no significant differences from 1.0 were found. In small bowel and peritoneum, mean THC ratios exceeded 1.0 before versus after PDT, and for small bowel, the ratio was signifi-

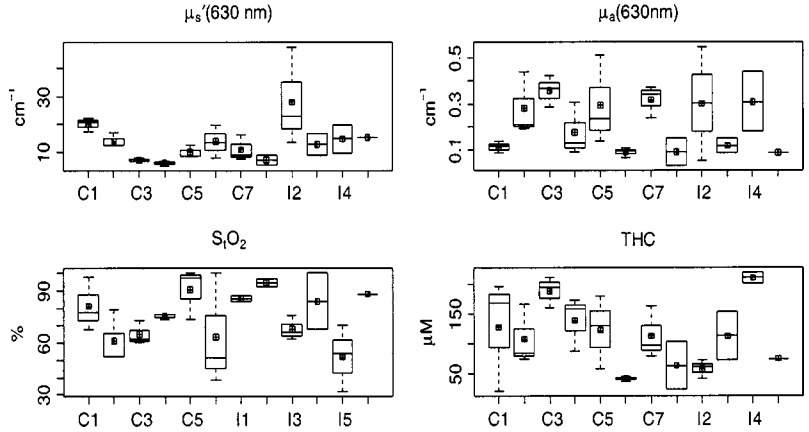

Fig. 4 Boxplots showing median (horizontal midline) and mean (squares) in $\mu_s'(\lambda=630\text{ nm})$, $\mu_a(\lambda=630\text{ nm})$, $\%S_tO_2$, and THC for three intraperitoneal sites (small and large bowel and peritoneum) in individual patients. Vertical lines extend to largest and smallest values for each patient and the box bisects the distance between the median and either the smallest or largest datapoint. The C series indicates patients with complete data from all five sites (intraperitoneal skin and liver); the I series indicate patients with incomplete data in at least one site.

Table 2 Means (SEM, standard error of the mean) of optical properties and physiological parameters for different normal tissues before and after PDT. Number of patients (n) used to calculate means and significant p-values (P) for global test of differences among at least one pair of tissues is shown. NS indicates a nonsignificant p-value, i.e., a p-value greater than 0.05. The parameter $c_{\text{Photofrin}}$ results for P (NS) were based only on intraperitoneal tissues.

Parameters	n	Small bowel	Large bowel	Peritoneum	Skin	Liver	P
				Before PDT			
μ_s' (630 nm) (cm^{-1})	7	10.05 (1.66)	10.42 (2.09)	14.28 (2.15)	13.60 (1.98)	27.53 (4.04)	0.004
μ_a (630 nm) (cm^{-1})	7	0.21 (0.04)	0.18 (0.04)	0.30 (0.06)	0.24 (0.06)	1.46 (0.16)	0.002
μ_{eff} (630 nm) (cm^{-1})	7	2.33 (0.22)	2.18 (0.25)	3.31 (0.35)	2.70 (0.51)	10.44 (0.51)	0.001
$\%S_tO_2$ (%)	6	65.8 (8.2)	87.7 (5.2)	64.9 (4.7)	70.8 (7.0)		0.013
THC (μM)	7	128.0 (26.0)	110.0 (17.0)	122.8 (28.0)	80.1 (33.5)		NS
$c_{\text{Photofrin}}$ (μM)	5	4.93 (2.3)	4.84 (2.3)	3.03 (1.0)	2.54 (0.94) (n=6)		NS
				After PDT			
μ_s' (630 nm) (cm^{-1})	4	8.95 (1.14)	10.11 (1.80)	15.99 (2.25)	18.05 (4.33)	28.76 (3.26)	0.031
μ_a (630 nm) (cm^{-1})	4	0.19 (0.06)	0.12 (0.04)	0.17 (0.06)	0.14 (0.09)	1.42 (0.12)	NS (P=0.006)
μ_{eff} (630 nm) (cm^{-1})	4	2.22 (0.46)	1.84 (0.48)	2.67 (0.61)	2.40 (1.08)	10.92 (0.20)	0.037
$\%S_tO_2$ (%)	3	59.4 (13.3)	67.8 (26.9)	88.1 (2.6)	72.5 (18.7)		NS
THC (μM)	3	52.9 (13.7)	65.9 (27.4)	69.0 (11.1)	66.8 (45.0)		NS
$c_{\text{Photofrin}}$ (μM)	3	3.36 (1.8)	2.04 (1.7)	0.4 (0.4)	5.04 (2.7) (n=5)		NS

cantly larger than 1.0 (P=0.013). For Photofrin, decreases in mean concentrations after-PDT compared to before-PDT ranged from 2.0 to 5.5 μM, and were significantly different from zero in the peritoneum (P=0.026).

3.5 *Differences between Normal and Tumor Intraperitoneal Tissues*

The optical and physiological properties of tumors from six patients, and their corresponding normal intraperitoneal tissues, are shown in Figs. 5 and 6, respectively. Table 4 shows the mean values of each parameter along with the mean of the individual tumor-to-normal tissue ratios for all parameters except $c_{\text{Photofrin}}$. For $c_{\text{Photofrin}}$, mean differences are shown. For the optical properties, μ_s' at 630 nm from tumors tended to be similar to normal small and large bowels, but significantly smaller than peritoneum (P=0.024). In contrast, μ_a and μ_{eff} at 630 nm from tumors tended to be somewhat higher than from normal intraperitoneal tissues, but the ratios were not significantly different from 1.0. The mean $\%S_tO_2$ in tumors was 33% with values ranging from 11 to 44%. The mean

Table 3 Mean (95% CI) of individual ratios of optical properties, $\%S_tO_2$ and THC in before- versus after-PDT measurements for patients with both measurements. For Photofrin, where the concentration was sometimes zero, we report a mean decrease in concentration before versus after PDT. A 95% CI on the mean ratio (mean difference) that does not cover 1.0 (0.0) is statistically different from a ratio of 1.0 (difference of 0.0). Note, the mean THC ratio is significantly different from 1.0, and the mean $c_{\text{Photofrin}}$ difference is significantly different from 0.0. ^{3}n=3, ^{4}n=4, ^{5}n=5, ^{6}n=6, ^{7}n=7, ^{8}n=8.

Parameters	Small bowel	Large bowel	Peritoneum	Skin	Liver
μ_s' (630 nm) ratio	0.96(0.7,1.4)^8	1.02(0.5,2.2)^5	0.88(0.4,2.0)^6	0.80(0.5,1.3)^8	1.00(0.6,1.8)^5
μ_a (630 nm) ratio	1.19(0.6,2.4)^8	0.85(0.2,4.1)^5	2.23(0.5,10.3)^6	1.94(0.5,7.5)^7	0.91(0.5,1.8)^5
μ_{eff} (630 nm) ratio	1.07(0.9,1.3)^8	0.93(0.3,2.5)^5	1.40(0.9,2.3,)^6	1.20(0.7,2.0)^7	0.95(0.8,1.1)^5
$\%S_tO_2$ ratio	1.23(0.9,1.8)^8	1.46(0.5,4.4,)^5	1.06(0.6,1.9)^6	1.09(0.6,1.9)^6	NA
THC ratio	5.29(1.7,16.5)^6	0.89(0.1,11.7)^3	2.67(0.5,14.0)^4	1.81(0.1,27.0)^4	NA
$\Delta c_{\text{Photofrin}}$ (μM)	2.56(−3.0,8.2)^6	5.48(−2.3,13.2)^3	2.27(0.5,4.0)^4	2.03(−1.8,5.8)^5	NA

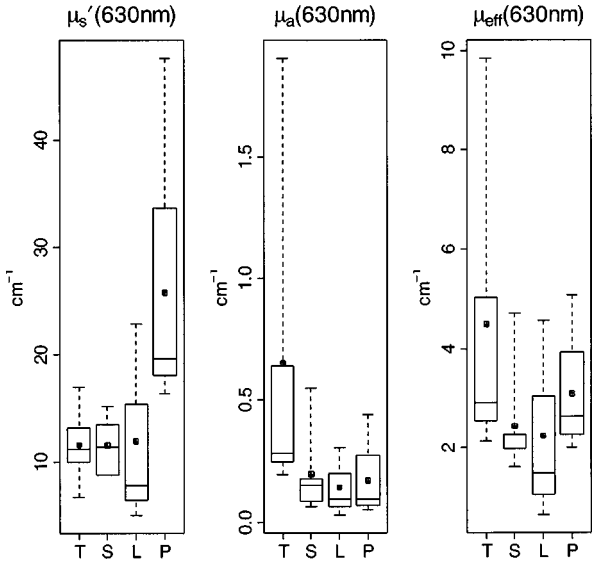

Fig. 5 Boxplots showing median (horizontal line) and means (squares) of optical properties for patients with measurements in both tumor (T) and intraperitoneal tissues (S small bowel, L large bowel, P peritoneum). Vertical dashed lines extend to largest and smallest values for each tissue, and the box indicates the interquartile range, roughly the middle half of the data.

$\%S_tO_2$ in tumors was significantly lower than those of the corresponding normal intraperitoneal tissues in the same patients for both small bowel and peritoneum ($P=0.018$ and $P=0.004$, respectively). The mean THC in tumor was 117 μM with values ranging from 61 to 224 μM, while mean Photofrin concentration was 7.4 μM with values ranging from 1.27 to 15.6 μM. Differences between THC and Photofrin in tumor and normal intraperitoneal tissues were not significant. However, for Photofrin, we noted the mean concentrations in tumor tended to be higher than for normal intraperitoneal tissues.

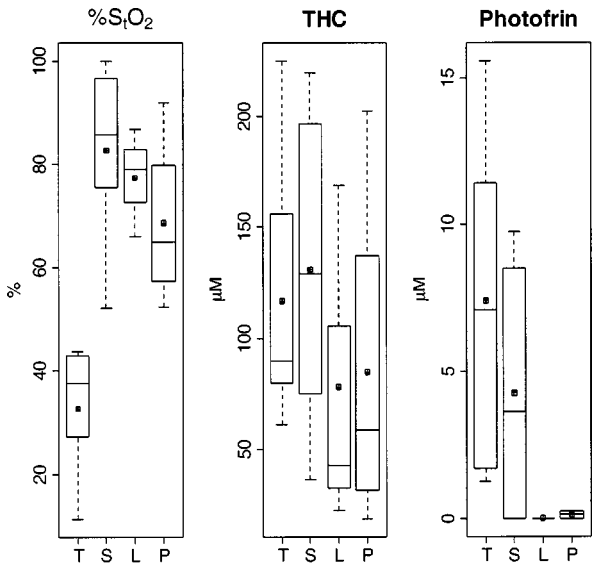

Fig. 6 Boxplots showing median (horizontal line) and means (squares) of physiologic properties for patients with measurements in both tumor (T) and intraperitoneal tissues (S small bowel, L large bowel, P peritoneum). Vertical dashed lines extend to largest and smallest values for each tissue, and the box indicates the interquartile range, roughly the middle half of the data.

4 Discussion

We have performed rapid, noninvasive measurements of optical and physiological properties in normal intraperitoneal tissues and tumors before and after PDT. The results demonstrate optical and physiological properties exhibit substantial inter- and intra-patient heterogeneity. Although a number of our findings are statistically significant, the small sample size may have limited our power to detect important differences in optical and/or physiological properties either among tissues, or in before versus after PDT measurements. In addition, comparison groups had variable numbers of subjects so that variation within the study in the ability to detect differences is also expected. For this reason, absence of statistically significant differences, e.g., Photofrin concentration in tumor versus normal tissues, post-PDT reduction in Photofrin concentration in normal tissues, should be interpreted cautiously. It is quite possible that studies with large patient groups might detect differences that were not conclusively demonstrated here. In addition, our sample of patients from this phase 2 clinical trial may not be representative of all patients with cancer, or even all patients with IP disease, so that further variation in optical and physiologic properties might occur as these types of measurements become available for other patient groups.

Our model assumed a semi-infinite homogeneous geometry for the tissues studied. This assumption is reasonable for normal intraperitoneal tissues and skin, because the surface areas of these tissues are generally at least twice as large as the size of the optical probes (approximately 1 cm in diameter) and the thickness of these tissues is greater than the sampling depth, which is approximately half of the source-detector separation distance used in this study [(1 to 5.2 mm)/2=0.5 to 2.6 mm]. Special care was taken by physicians while taking the measurements to very lightly touch the optical probes on the central surface of the tissue interested. The assumption of homogeneity is probably not as good as the semi-infinite assumption, but it is the only reasonable approach to take given lack of precise information about tissue heterogeneity. In two of nine tumor nodules, their sizes (width $\times$length) were recorded to be 6×7 mm^2 and 11.5×7 mm^2, respectively, from the surface of the small bowel. For the remaining tumor nodules, physicians intentionally selected tumors with diameters greater than 5 mm and less than 1 cm for the measurements. Although the tissue surface area is approximately the same as our optical probes, the source-detector separation distances used to analyze these tumor tissue data were typically less than 3 mm. Therefore, the assumption of semi-infinite turbid media in our model is reasonably good.

In our current analytical model, we observed 2 to 4 times higher fitting error (defined before) with the liver data (5 to 8% fitting error using minimal two source separation distances 1 to 3 mm) compared to the errors encountered during analysis of other intraperitoneal tissues (typically $<2\%$). We were unable to extract oxygenation and THC information from liver tissues for the following reasons. First, liver has a

Table 4 Left: means (95% CI) of optical and physiological properties for tumor tissues. Right: ratios of tumor to normal intraperitoneal tissues for optical parameters, $\%S_tO_2$ and THC; difference between tumor and normal tissue for $c_{Photofrin}$. Note that a 95% CI on the mean ratio (difference) that does not include 1.0 (or 0.0 for Photofrin) is statistically different from 1.0 (0.0). NA indicates insufficient n to construct a 95% CI, i.e., n≤2. [1]n=1, [2]n=2, [3]n=3, [4]n=4, [5]n=5, [6]n=6; * statistically different from 1.0.

		Mean of ratios (difference) for comparison group (95% CI)		
Parameters	Tumor	Small bowel	Large bowel	Peritoneum
μ_s' (630 nm) (cm^{-1})	11.6(6.9,16.3)[5]	0.94(0.7,1.3)[5]	0.86(NA)[2]	0.43(0.2,0.8)[4]*
μ_a (630 nm) (cm^{-1})	0.65(0.0,1.5)[5]	2.87(0.6,13.5)[5]	2.51(NA)[2]	2.53(0.3,18.7)[4]
μ_{eff} (630 nm) (cm^{-1})	4.49(0.5,8.4)[5]	1.63(0.7,3.7)[5]	1.47(NA)[2]	1.03(0.4,2.8)[4]
$\%S_tO_2$ (%)	32.6(15.8,49.5)[5]	0.37(0.2,0.8)[5]*	0.44(NA)[2]	0.56(0.4,0.7)[4]*
THC (μM)	116.8(52,181)[6]	0.95(0.4,2.0)[6]	1.87(0.1,51.7)[3]	1.65(0.5,5.1)[4]
$c_{Photofrin}$ (μM)	7.4(0,15.1)[5]	3.24(−10.6,16.8)[4]	1.27(NA)[1]	4.01(NA)[2]

high hemoglobin concentration, and therefore a high absorption coefficient such that the diffusion theory may not hold.[37] Second, the assumption that μ_a is composed of four chromophores (HbO_2, Hb, Photofrin, and water) may not apply to liver. Other chromophores, such as fat and pigments, may need to be included in this model. With these caveats, however, we were still able to estimate μ_s', μ_a, μ_{eff}, and penetration depth in this study based on our model. The mean values (±SEM, *n*) of penetration depths in liver, derived from μ_{eff}, were 0.95 (±0.06, 6) mm before PDT and 0.92 (±0.02, 4) mm after PDT. These values are comparable with an *in-vitro* study, which showed the penetration depth was 1 to 2 mm using a double integrating sphere system.[65] The significant low penetration depth in liver was contributed to by both higher μ_s' and μ_a, as compared to other tissues measured in this study.

For other tissues, the mean (±SEM, *n*) of the penetration depths in millimeters, derived from μ_{eff}, were 4.78 (±0.6, 6), 5.20 (±0.67, 6), 3.39 (±0.29, 6), 5.19 (±1.40, 6), and 3.02 (±0.66, 5) for small bowel, large bowel, peritoneum, skin, and tumor, respectively. These results fall into reasonable ranges compared to published *in-vivo* human studies in other tissues, for example brain,[44,45] breast tumors,[46] prostatic carcinoma,[47] and esophageal carcinoma.[48,49] Wilson et al. reported a penetration depth of 0.8 to 4.9 mm in brain tumors of six patients and 1.0 to 1.7 mm in normal brain tissue of two patients. Driver, Lowdell, and Ash reported the penetration depths of breast tumors from four patients to be 2.9 to 4.7 mm. Lee et al. reported a penetration depth of 2.98±0.78 mm in prostatic carcinoma. And Maier et al. measured the penetration depth of esophageal carcinoma to be 2.68 to 3.21 mm and found that the penetration depth tended to decrease as the tumor diameter increased. Bays et al. obtained $\mu_{eff}(\lambda = 630\,nm) = 0.24 \pm 0.1\,mm^{-1}$ and $\mu_s'(\lambda = 630\,nm) = 0.70 \pm 0.23\,mm^{-1}$ from 51 measurements of the esophagus of 11 patients. Tumors tend to have lower penetration depth than small and large bowel. This is likely due to higher absorption in tumors due to lower oxygenation and higher total hemoglobin concentration.

Peritoneum showed optical properties similar to skin, but unexpectedly lower penetration depth, compared to small and large bowel. Peritoneum is a thin connective tissue layer lined by mesothelium. The tissues underlying the peritoneum are normally connective tissue, fat, and muscle. Therefore, it is structurally similar to skin. It is not surprising that peritoneum has similar μ_s' to skin. However, the significantly lower penetration depth in peritoneum compared to small and large bowel may be due to higher blood content on the surface of the peritoneum during a surgical operation.

The values of $\%S_tO_2$ of 32 to 100% and THC of 19 to 263 μM in normal and tumor tissues lie within the expected physiological ranges. Tumor has a $\%S_tO_2$ of 11 to 44% that is significantly lower than the corresponding intraperitoneal tissues from the same patients, and a wide range of THC of 61 to 224 μM. Other studies have reported $\%S_tO_2$ and THC in normal and tumor tissues using NIR spectroscopy and/or DOT techniques in breast[29–31,42,43] and colon.[40] Durduran et al. measured $\%S_tO_2$ and THC in breast tissue from 52 normal subjects to have mean (±SD) 68 (±8)% and 34 (±9) μM, respectively. Tromberg et al. showed that, from three subjects, normal breast tissue had $\%S_tO_2$ and THC ~80%, and 20 μM, respectively, and tumor had lower $\%S_tO_2$ (~65%) and higher THC (35 μM) than normal tissue. Subhadra et al. acquired measurements in breast tissues from 24 healthy subjects and reported $\%S_tO_2$ and THC to have mean (±SD) 58 (±9)% and 22 (±8) μM with ranges of 32 to 75% and 9 to 41 μM, respectively. Pogue et al. reported typical values for THC ranging from 10 to 60 μM by imaging the whole breast from a frequency-domain system. Quaresima et al. reported measurements of $\%S_tO_2$ and THC in the breasts of five subjects to have ranges of 0 to 90% and 2.9 to 20.4 μM, respectively. Zonios et al. reported from 13 patients that normal colon mucosal tissues had mean (±SD) of $\%S_tO_2$ and THC 65 (±5)% and 22.5 (±2) mg/dL (~14 μM), respectively, and polyps had similar $\%S_tO_2$ (55±5%) and six times higher THC (165±22 mg/dL≈100 μM) than normal mucosal tissues.

It is known that some tumors exhibit features of increased microvasculature, hence increased blood content,[66] and that some tumors are characterized by hypoxia.[67] Our results show that $\%S_tO_2$ in tumor is significantly lower than the corresponding normal intraperitoneal tissues, but the differences in THC between tumor and normal tissues were not statistically significant. This is possibly due to small sample size in the study, as described previously, or because the patients that were used to make the comparison for $\%S_tO_2$ were not identical to the ones used to make the THC comparison. There were some differences observed in the patients that were used in the two comparisons. However, when we used only the patients in common to the two comparisons, there was no obvious relationship between $\%S_tO_2$ and THC before PDT in five samples that were collected from the same patients.

Mean Photofrin concentrations ranged from 2.5 to 4.9 μM before PDT and from 0.4 to 5.0 μM after PDT (Table 2). Mean Photofrin concentration consistently decreased in all tissues after PDT, significantly in peritoneum (Table 3). This decrease after PDT is likely due to photobleaching that has been observed in other PDT studies.[68] Photofrin concentrations were not extracted successfully in every tissue, possibly due to its lower μ_a compared to oxy- and deoxy-hemoglobin and its similar spectral shape to deoxy-hemoglobin. In instances where the Photofrin measurements reached the upper boundary value (40 μM) that was set in the algorithm, the data were treated as not evaluable. In these cases, we found the true Photofrin concentration did not affect the accuracy of μ_s', μ_a, μ_{eff}, THC, and $\%S_tO_2$ (within 3% CV) (data not shown).

In this study, we detected large heterogeneity among patients as well as trends in optical and physiological properties between normal and tumor tissues, before and after PDT in normal tissues, and between various normal tissue types. The large heterogeneity among and within patients suggests the need for real-time dosimetry during PDT to optimize the treatment condition, depending on the optical and physiological properties that are measured from site to site.

5 Conclusion

The optical and physiological properties of 12 patients with intraperitoneal malignancies are measured, before and after PDT treatment, using a broadband diffuse reflectance spectroscopy system. The analysis is done with a fast algorithm to extract important dosimetric quantities simultaneously such as oxygen saturation, photosensitizer concentration, and light penetration depth. We observed substantial heterogeneity in optical and physiological property measurements. The optical and physiological properties varied from site to site, tissue to tissue, and patient to patient. Optical and physiological properties are similar before and after PDT except for Photofrin, which tends to decrease after PDT, possibly due to photobleaching. As expected, tumors tend to have lower oxygenation, higher drug uptake, and lower penetration depth compared to normal intraperitoneal tissues.

Acknowledgments

We acknowledge useful discussions with R. Choe, J. Zhang, T. Durduran, J. Giammarco, and J. Finlay for the design of tissue phantom experiments and the development of the algorithm. We also thank C. J. Koch and T. M. Busch who provided the oxygen electrode probe and thoughtful discussions about out validating $\%S_tO_2$ measurements. This work is supported by NIH PO1 grant CA87971.

References

1. T. J. Dougherty, C. J. Gomer, B. W. Henderson, G. Jori, D. Kessel, M. Korbelik, J. Moan, and Q. Peng, ''Photodynamic therapy,'' *J. Natl. Cancer Inst.* **90**(12), 889–905 (1998).
2. S. M. Hahn and E. Glatstein, ''The emergence of photodynamic therapy as a major modality in cancer treatment,'' *Rev. Contemp. Pharmacotherapy* **10**(1), 69–74 (1999).
3. T. J. Dougherty, M. T. C. Cooper, and T. S. Mang, ''Cutaneous phototoxic occurrences in patients receiving Photofrin,'' *Lasers Surg. Med.* **10**(5), 485–488 (1990).
4. V. M. Mullooly, A. L. Abramson, and M. J. Shikowitz, ''Dihematoporphyrin ether-induced photosensitivity in laryngeal papilloma patients,'' *Lasers Surg. Med.* **10**(4), 349–356 (1990).
5. G. Wagnieres, C. Hadjur, P. Grosjean, D. Braichotte, J. F. Savary, P. Monnier, and H. van den Bergh, ''Clinical evaluation of the cutaneous phototoxicity of 5, 10, 15, 20-tetra (m-hydroxyphenyl)chlorin,'' *Photochem. Photobiol.* **68**(3), 382–387 (1998).
6. T. J. Panella, T. J. Wieman, and S. E. A. Dougherty, ''Lutetium texaphyrin (Lu-Tex) photodynamic therapy (PDT) of patients with refractory locally recurrent breast cancer,'' *Proc. Am. Soc. Clin. Oncol.* **17**, 165 (1998).
7. W. E. Grant, C. Hopper, P. M. Speight, M. R. C. Path, A. J. MacRobert, and S. G. Brown, ''Photodynamic therapy of malignant and premalignant lesions in patients with 'field cancerization' of the oral cavity,'' *J. Laryngol. Otol.* **107**(12), 1140–1145 (1993).
8. H. Barr, N. A. Shepherd, A. Dix, D. J. H. Roberts, W. C. Tan, and N. Krasner, ''Eradication of high-grade dysplasia in columnar-lined (Barrett's) oesophagus by photodynamic therapy with endogenously generated protoporphyrin IX,'' *Lancet* **348**(9027), 584–585 (1996).
9. B. F. Overholt and M. Panjiehpour, ''Photodynamic therapy in Barrett's esophagus: Clinical update,'' *Am. J. Gastroenterol.* **91**(9), 1719–1723 (1996).
10. H. Takita, T. S. Mang, G. M. Loewen, J. G. Antkowlak, D. Raghavan, J. R. G. Grajek, and T. J. Dougherty, ''Operation and intracavitary photodynamic therapy for malignant pleural mesothelioma: a phase II study,'' *Ann. Thorac. Surg.* **58**(4), 995–998 (1994).
11. H. I. Pass and J. S. Donington, ''Use of photodynamic therapy for the management of pleural malignancies,'' *Semin. Surg. Oncol.* **11**(5), 360–367 (1995).
12. J. Friedberg, R. Mick, J. Stevenson, J. Metz, T. Zhu, J. Buyske, D. H. Sterman, H. I. Pass, E. Glatstein, and S. M. Hahn, ''A phase I study of foscan-mediated photodynamic therapy and surgery in patients with mesothelioma,'' *Ann. Thorac. Surg.* **75**(3), 952–959 (2003).
13. T. F. DeLaney, W. F. Sindelar, Z. Tochner, P. D. Smith, W. S. Friauf, G. Thomas, L. Dachowski, J. W. Cole, S. M. Steinberg, and E. Glatstein, ''Phase-I study of debulking surgery and photodynamic therapy for disseminated intraperitoneal tumors,'' *Int. J. Radiat. Oncol., Biol. Phys.* **25**(3), 445–457 (1993).
14. S. K. Hendren, S. M. Hahn, F. R. Spitz, T. W. Bauer, S. C. Rubin, T. Zhu, E. Glatstein, and D. L. Fraker, ''Phase II trial of debulking surgery and photodynamic therapy for disseminated intraperitoneal tumors,'' *Ann. Surg. Oncol.* **8**(1), 65–71 (2001).
15. T. W. Bauer, S. M. Hahn, F. R. Spitz, A. Kachur, E. Glatstein, and D. L. Fraker, ''Preliminary report of phyotodynamic therapy for intraperitoneal sarcomatosis,'' *Ann. Surg. Oncol.* **8**(3), 254–259 (2001).
16. N. L. Oleinick and H. H. Evans, ''The photobiology of photodynamic therapy: cellular targets and mechanisms,'' *Radiat. Res.* **150**(5), S146–156 (1998).
17. C. J. Gomer and N. J. Razum, ''Acute skin-response in albino mice following porphyrin photosensitization under oxic and anoxic conditions,'' *Photochem. Photobiol.* **40**(4), 435–439 (1984).
18. J. Moan and S. Sommer, ''Oxygen dependence of the photosensitizing effect of hematoporphyrin derivative in NHIK 3025 cells,'' *Cancer Res.* **45**(4), 1608–1610 (1985).
19. B. W. Henderson, T. M. Busch, L. A. Vaughan, N. P. Frawley, D. Babich, T. A. Sosa, J. D. Zollo, A. S. Dee, M. T. Cooper, D. A. Bellnier, W. R. Greco, and A. R. Oseroff, ''Photofrin photodynamic therapy can significantly deplete or preserve oxygenation in human

basal cell carcinomas during treatment, depending on fluence rate,'' *Cancer Res.* **60**(3), 525–529 (2000).
20. I. J. MacDonald and T. J. Dougherty, ''Basic principles of photodynamic therapy,'' *J. Porphyrins Phthalocyanines* **5**(2), 105–129 (2001).
21. B. C. Wilson, M. S. Patterson, and L. Lilge, ''Implicit and explicit dosimetry in photodynamic therapy: a new paradigm,'' *Lasers Med. Sci.* **12**(3), 182–199 (1997).
22. A. G. Yodh and D. A. Boas, ''Functional imaging with diffusing light,'' Chap. 21 in *Biomedical Photonics Handbook*, pp. 21-21–21-45, CRC Press, Boca Raton, FL (2003).
23. R. Choe, T. Durduran, G. Q. Yu, M. J. M. Nijland, B. Chance, A. G. Yodh, and N. Ramanujam, ''Transabdominal near infrared oximetry of hypoxic stress in fetal sheep brain in utero,'' *Proc. Natl. Acad. Sci. U.S.A.* **100**(22), 12950–12954 (2003).
24. T. H. Pham, R. Hornung, M. W. Berns, Y. Tadir, and B. J. Tromberg, ''Monitoring tumor response during photodynamic therapy using near-infrared photon-migration spectroscopy,'' *Photochem. Photobiol.* **73**(6), 669–677 (2001).
25. A. Sassaroli, F. Martelli, Y. Tanikawa, K. Tanaka, R. Araki, Y. Onodera, and Y. Yamada, ''Time-resolved measurements of in vivo optical properties of piglet brain,'' *Opt. Rev.* **7**(5), 420–425 (2000).
26. Y. Du, X. H. Hu, M. Cariveau, X. Ma, G. W. Kalmus, and J. Q. Lu, ''Optical properties of porcine skin dermis between 900 nm and 1500 nm,'' *Phys. Med. Biol.* **46**(1), 167–181 (2001).
27. T. C. Zhu, S. M. Hahan, A. S. Kapatkin, A. Dimofte, C. E. Rodriguez, T. G. Vulcan, E. Glatstein, and R. A. Hsi, ''In vivo optical properties of normal canine prostate at 732 nm using motexafin lutetium-mediated photodynamic therapy,'' *Photochem. Photobiol.* **77**(1), 81–88 (2003).
28. T. Kital, B. Beauvoit, and B. Chance, ''Optical determination of fatty change of the graft liver with near-infrared time-resolved spectroscopy,'' *Transplantation* **62**(5), 642–647 (1996).
29. B. J. Tromberg, N. Shah, R. Lanning, A. Cerussi, J. Espinoza, T. H. Pham, L. Svaasand, and J. Butler, ''Non-invasive in vivo characterization of breast tumors using photon migration spectroscopy,'' *Neoplasia* **2**(1,2), 26–40 (2000).
30. T. Durduran, R. Choe, J. P. Culver, L. Zubkov, M. J. Holboke, J. Giammarco, B. Chance, and A. G. Yodh, ''Bulk optical properties of healthy female breast tissue,'' *Phys. Med. Biol.* **47**(16), 2847–2861 (2002).
31. S. Srinivasan, B. W. Pogue, S. D. Jiang, H. Dehghani, C. Kogel, S. Soho, J. J. Gibson, T. D. Tosteson, S. P. Poplack, and K. D. Paulsen, ''Interpreting hemoglobin and water concentration, oxygen saturation, and scattering measured in vivo by near-infrared breast tomography,'' *Proc. Natl. Acad. Sci. U.S.A.* **100**(21), 12349–12354 (2003).
32. N. Shah, A. Cerussi, C. Eker, J. Espinoza, J. Bulter, J. Fishkin, R. Hornung, and B. J. Tromberg, ''Noninvasive functional optical spectroscopy of human breast tissue,'' *Proc. Natl. Acad. Sci. U.S.A.* **98**(8), 4420–4425 (2001).
33. F. Bevilacqua, D. Poiguet, P. Marquet, J. D. Gross, B. J. Tromberg, and C. Depeursinge, ''In vivo local determination of tissue optical properties: applications to human brain,'' *Appl. Opt.* **38**(22), 4939–4950 (1999).
34. J. C. Hebden, A. Gibson, R. M. Yusof, N. Everdell, E. M. C. Hillman, D. T. Delpy, S. R. Arridge, T. Austin, J. H. Meek, and J. S. Wyatt, ''Three-dimensional optical tomography of the premature infant brain,'' *Phys. Med. Biol.* **47**(23), 4155–4166 (2002).
35. N. Dognitz and G. Wagnieres, ''Determination of tissue optical properties by steady-state spatial frequency-domain reflectometry,'' *Lasers Med. Sci.* **13**(1), 55–65 (1998).
36. E. M. C. Hillman, J. C. Hebden, M. Schweiger, H. Dehghani, F. E. W. Schmidt, D. T. Delpy, and S. R. Arridge, ''Time resolved optical tomography of the human forearm,'' *Phys. Med. Biol.* **46**(4), 1117–1130 (2001).
37. J. B. Fishkin, S. Fantini, M. J. vandeVen, and E. Gratton, ''Gigahertz photon density wave in a turbid medium: Theory and experiments,'' *Phys. Rev. E* **53**(3), 2307–2319 (1996).
38. J. R. Mourant, I. J. Bigio, J. Boyer, T. Johnson, and J. Lacey, ''Detection of GI cancer by elastic scattering spectroscopy,'' *J. Biomed. Opt.* **1**(2), 192–199 (1996).
39. J. R. Mourant, I. J. Bigio, J. Boyer, R. L. Conn, R. Johnson, and T. Shimada, ''Spectroscopic diagnosis of bladder cancer with elastic light scattering,'' *Lasers Surg. Med.* **17**(4), 350–357 (1995).
40. G. Zonios, L. T. Perelman, V. M. Backman, R. Manoharan, M. Fitzmaurice, J. van Dam, and M. S. Feld, ''Diffuse reflectance spectroscopy of human adenomatous colon polyps in vivo,'' *Appl. Opt.* **38**(31), 6628–6637 (1999).
41. Y. N. Mirabal, S. K. Chang, E. N. Atkinson, A. Malpica, M. F. Follen, and R. Richards-Kortum, ''Reflectance spectroscopy for in vivo detection of cervical precancer,'' *J. Biomed. Opt.* **7**(4), 587–594 (2002).
42. B. W. Pogue, S. P. Poplack, T. O. McBride, W. A. Wells, K. S. Osterman, U. L. Osterberg, and K. D. Paulsen, ''Quantitative hemoglobin tomography with diffuse near-infrared spectroscopy: Pilot results in the breast,'' *Radiol.* **218**(1), 261–266 (2001).
43. V. Quaresima, S. J. Matcher, and M. Ferrari, ''Identification and quantification of intrinsic optical contrast for near-infrared mammography,'' *Photochem. Photobiol.* **67**(1), 4–14 (1998).
44. B. C. Wilson, P. J. Muller, and J. C. Yanch, ''Instrumentation and light dosimetry for intra-operative photodynamic therapy (PDT) of malignant brain tumors,'' *Phys. Med. Biol.* **31**(2), 125–133 (1986).
45. P. J. Muller and B. C. Wilson, ''An update on the penetration depth of 630 nm light in normal and malignant human-brain tissue in vivo,'' *Phys. Med. Biol.* **31**(11), 1295–1297 (1986).
46. I. Driver, C. P. Lowdell, and D. V. Ash, ''In vivo measurement of the optical interaction coefficients of human tumors at 630 nm,'' *Phys. Med. Biol.* **36**(6), 805–813 (1991).
47. L. K. Lee, C. Whitehurst, M. L. Pantelides, and J. V. Moore, ''An interstitial light assembly for photodynamic therapy in prostatic carcinoma,'' *BJU Intl.* **84**(7), 821–826 (1999).
48. A. Maier, D. Sullmann, U. Anegg, F. Tomaselli, P. Rehak, H. Hutten, H. Pinter, and F. M. Smolle-Juttner, ''In vivo determination of tumor optical parameters in esophageal carcinoma,'' *Lasers Surg. Med.* **27**(4), 350–357 (2000).
49. R. Bays, G. Wagnieres, D. Robert, D. Braichotte, J. F. Savary, P. Monnier, and H. vandenBergh, ''Clinical determination of tissue optical properties by endoscopic spatially resolved reflectometry,'' *Appl. Opt.* **35**(10), 1756–1766 (1996).
50. M. Solonenko, R. Cheung, T. M. Busch, A. Kachur, G. M. Griffin, T. Vulcan, T. C. Zhu, H. W. Wang, S. M. Hahn, and A. G. Yodh, ''In vivo reflectance measurement of optical properties, blood oxygenation and motexafin lutetium uptake in canine large bowels, kidneys, and prostates,'' *Phys. Med. Biol.* **47**(6), 857–873 (2002).
51. E. L. Hull, M. G. Nichols, and T. H. Foster, ''Quantitative broadband near-infrared spectroscopy of tissue-simulating phantoms containing erythrocytes,'' *Phys. Med. Biol.* **43**(11), 3381–3404 (1998).
52. B. C. Wilson, T. J. Farrell, and M. S. Patterson, ''An optical fiber-based diffuse reflectance spectrometer for non-invasive investigation of photodynamic sensitizers in vivo,'' *Proc. SPIE* **6**, 219–232 (1990).
53. E. L. Hull, M. G. Nichols, and T. H. Foster, ''Localization of luminescent inhomogeneities in turbid media with spatially resolved measurements of CW diffuse luminescence emittance,'' *Appl. Opt.* **37**(13), 2755–2765 (1998).
54. R. C. Haskell, L. O. Svaasand, T. T. Tsay, T. C. Feng, M. S. McAdams, and B. J. Tromberg, ''Boundary conditions for the diffusion equation in radiative transfer,'' *J. Opt. Soc. Am. A* **11**(10), 2727–2741 (1994).
55. T. J. Farrell, M. S. Patterson, and B. C. Wilson, ''A diffusion theory model of spatially resolved, steady-state diffuse reflectance for the noninvasive determination of tissue optical properties in vivo,'' *Med. Phys.* **19**(4), 879–888 (1992).
56. A. Kienle and M. S. Patterson, ''Improved solutions of the steady-state and the time-resolved diffusion equations for reflectance from a semi-infinite turbid medium,'' *J. Opt. Soc. Am. A* **14**(1), 246–254 (1997).
57. A. Kienle and M. S. Patterson, ''Determination of the optical properties of semi-infinite turbid media from frequency-domain reflectance close to the source,'' *Phys. Med. Biol.* **42**(9), 1801–1819 (1997).
58. A. Corlu, T. Durduran, R. Choe, M. Schweiger, E. M. C. Hillman, S. R. Arrige, and A. G. Yodh, ''Uniqueness and wavelength optimization in continuous-wave multispectral diffuse optical tomography,'' *Opt. Lett.* **28**(23), 2339–2341 (2003).
59. S. A. Prahl, ''Optical properties spectra,'' see http://omic.ogi.edu/spectra/index.html (2001).
60. H. J. van Staveren, C. J. M. Moes, J. van Marie, S. A. Prahl, and M. J. C. van Gemert, ''Light scattering in Intralipid-10% in the wavelength range of 400–1100 nm,'' *Appl. Opt.* **30**(31), 4507–4514 (1991).
61. J. R. Mourant, T. Fuselier, J. Boyer, T. M. Johnson, and I. J. Bigio, ''Predictions and measurements of scattering and absorption over

broad wavelength ranges in tissue phantoms,'' *Appl. Opt.* **36**(4), 949–957 (1997).
62. R. Ihaka and R. R. Gentleman, ''R: A language for data analysis and graphics,'' *J. Graph. Comput. Stat.* **5**, 299–314 (1996).
63. M. Hollander and D. Wolfe, *Nonparametric Statistical Methods*, John Wiley and Sons, New York (1999).
64. B. D. Marx and P. H. C. Eilers, ''Generalized linear regression on sampled signals and curves: A p-spline approach,'' *Technometrics* **41**(1), 1–13 (1999).
65. J. P. Ritz, A. Roggan, C. Isbert, G. Muller, H. J. Buhr, and C. T. Germer, ''Optical properties of native and coagulated porcine liver tissue between 400 and 2400 nm,'' *Lasers Surg. Med.* **29**(3), 205–212 (2001).
66. R. K. Jain, ''Determinants of tumor blood flow: a review,'' *Cancer Res.* **48**(10), 2641–2658 (1988).
67. P. Vaupel, ''Oxygen transport in tumors: characteristics and clinical implications,'' *Adv. Exp. Med. Biol.* **388**, 341–351 (1996).
68. V. X. D. Yang, P. J. Muller, P. Herman, and B. C. Wilson, ''A multispectral fluorescence imaging system: design and initial clinical tests in intra-operative Photofrin-photodynamic therapy of brain tumors,'' *Lasers Surg. Med.* **32**(3), 224–232 (2003).